

Avondale College

ResearchOnline@Avondale

Science and Mathematics Papers and Journal
Articles

Faculty of Science and Mathematics

12-6-2007

Rationalizing the Different Products in the Reaction of N₂ with Three-coordinate MoL₃ Complexes

Gemma J. Christian

Avondale College, gemma.christian@avondale.edu.au

Robert Stranger

Australian National University


Brian F. Yates

University of Tasmania

Christopher C. Cummins

Massachusetts Institute of Technology

Follow this and additional works at: https://research.avondale.edu.au/sci_math_papers

 Part of the [Chemistry Commons](#)

Recommended Citation

Christian, G., Stranger, R., Yates, B. F., & Cummins, C. C. (2007). Rationalizing the different products in the reaction of N₂ with three-coordinate MoL₃ complexes. *Dalton Transactions*, 2007(19), 1939–1947. doi:10.1039/B701050H

This Article is brought to you for free and open access by the Faculty of Science and Mathematics at ResearchOnline@Avondale. It has been accepted for inclusion in Science and Mathematics Papers and Journal Articles by an authorized administrator of ResearchOnline@Avondale. For more information, please contact alicia.starr@avondale.edu.au.

Rationalizing the different products in the reaction of N₂ with three-coordinate MoL₃ complexes†

Gemma Christian,^a Robert Stranger,^{*a} Brian F. Yates^b and Christopher C. Cummins^c

Received 23rd January 2007, Accepted 9th March 2007

First published as an Advance Article on the web 26th March 2007

DOI: 10.1039/b701050h

The reaction of N₂ with three-coordinate MoL₃ complexes is known to give rise to different products, N–MoL₃, L₃Mo–N–MoL₃ or Mo₂L₆, depending on the nature of the ligand L. The energetics of the different reaction pathways are compared for L = NH₂, NMe₂, N(ⁱPr)Ar and N(^tBu)Ar (Ar = 3,5-C₆H₃Me₂) using density functional methods in order to rationalize the experimental results. Overall, the exothermicity of each reaction pathway decreases as the ligand size increases, largely due to the increased steric crowding in the products compared to reactants. In the absence of steric strain, the formation of the metal–metal bonded dimer, Mo₂L₆, is the most exothermic pathway but this reaction shows the greatest sensitivity to ligand size varying from significantly exothermic, –403 kJ mol^{–1} for L = NMe₂, to endothermic, +78 kJ mol^{–1} for L = N(^tBu)Ar. For all four ligands, formation of N–MoL₃ via cleavage of the N₂ bridged dimer intermediate, L₃Mo–N–N–MoL₃, is strongly exothermic. However, in the presence of excess reactant MoL₃, formation of the single atom-bridged complex L₃Mo–N–MoL₃ from N–MoL₃ + MoL₃ is both thermodynamically and kinetically favoured for L = NMe₂ and N(ⁱPr)Ar, in agreement with experiment. In the case of L = N(^tBu)Ar, the greater steric bulk of the ^tBu group results in a much less exothermic reaction and a calculated barrier of 66 kJ mol^{–1} to formation of the L₃Mo–N–MoL₃ dimer. Consequently, for this ligand, the energetically and kinetically favoured product, consistent with the experimental data, is the nitride complex L₃Mo–N.

Introduction

The high temperatures (400–550 °C) and pressures (100–300 atm) necessary to drive the Haber–Bosch process, the main commercial route to producing ammonia from N₂, have prompted significant efforts to develop transition metal systems that are capable of activating and cleaving dinitrogen under mild conditions.^{1–6} On this theme, the three-coordinate complex Mo[N(R)Ar]₃ (R = ^tBu, Ar = 3,5-C₆H₃Me₂) is well known for its ability to bind and cleave N₂ at ambient temperature and pressure.^{7,8} Since the initial

discovery of this remarkable reaction, a range of M[N(R)Ar]₃ complexes have been made with other metals and bulky amide ligands N(R)Ar, including M = Ti, Cr, Fe and V,^{9–14} R = Me, ⁱPr, ^tBu, 1-Ad and 2-Ad (Ad = Adamantyl) and Ar = Me, Ph and 3,5-C₆H₃Me₂. In addition, X–M[N(R)Ar]₃ halide complexes have been synthesised for M = Mo, Sn, Nb and U and X = Cl, Br or I.^{15,16,17–19} In general, these complexes are very sensitive to both the identity of the metal and the amide ligand, in particular its size, and varying either can have a significant effect on the products formed on reaction with N₂.

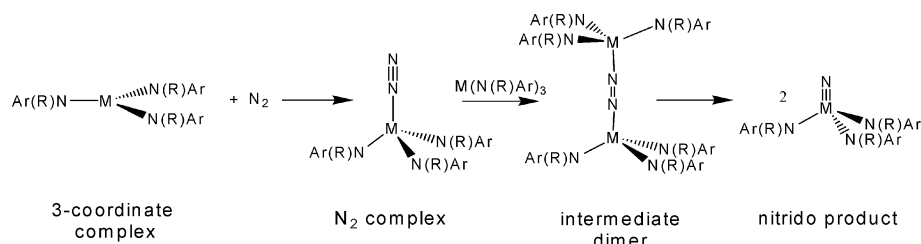
There have been several experimental^{8,14,20} and theoretical^{21–23} studies of the reaction of Mo[N(^tBu)Ar]₃ with N₂ and the mechanism of the reaction is now well established. The first step in the reaction is the coordination of N₂ to Mo[N(^tBu)Ar]₃ as shown in Scheme 1 to form N₂–Mo[N(^tBu)Ar]₃. This is followed by coordination of a second Mo[N(^tBu)Ar]₃ to form an intermediate dimer with N₂ bridging end-on to both Mo centres. The dinitrogen bond then cleaves to form the nitrido product N–Mo[N(^tBu)Ar]₃. The barrier to cleavage has been measured at 97 kJ mol^{–1}⁸ and the overall reaction is calculated to be exothermic by around 300 kJ mol^{–1}.²¹

^aDepartment of Chemistry, Faculty of Science, Australian National University, Canberra, ACT, 0200, Australia. E-mail: rob.stranger@anu.edu.au

^bSchool of Chemistry, University of Tasmania, Private Bag 75, Hobart, TAS, 7001, Australia

^cDepartment of Chemistry, Massachusetts Institute of Technology, Cambridge, MA, 02139, USA

† Electronic supplementary information (ESI) available: Energies and cartesian coordinates for the optimised structures of MoL₃, N–MoL₃, Mo₂L₆ and L₃Mo–N–MoL₃ for L = NH₂, NMe₂, N(ⁱPr)Ar and N(^tBu)Ar. Linear transit data for the rotation around the central Mo–Mo bond in Mo₂L₆ for L = NH₂. See DOI: 10.1039/b701050h



Scheme 1 Reaction mechanism for N₂ cleavage by Mo[N(R)Ar]₃.

The $\text{Mo}[\text{N}(\text{R})\text{Ar}]_3$ complex has approximately C_3 symmetry as shown in Fig. 1, with the R substituents and Ar groups arranged on opposite sides of the trigonal MoN_3 plane. The steric bulk of the $\text{N}(\text{R})\text{Ar}$ ligands is important in stabilizing the low coordination number of the metal which in turn enhances the reactivity of these complexes towards small molecules. Small molecules are able to bind to the Mo center *via* the channel between the R groups but the size of the incoming molecule is restricted by the steric bulk of the R substituents. Dimerisation to form the very stable metal–metal bonded dimer, $\text{Mo}_2[\text{N}(\text{R})\text{Ar}]_6$, is also prevented when the R groups are sufficiently large. Thus, the combination of coordinative unsaturation and restricted access to the metal makes these sterically-encumbered, three-coordinate complexes ideal for binding and activating small, multiply-bonded molecules such as N_2 .

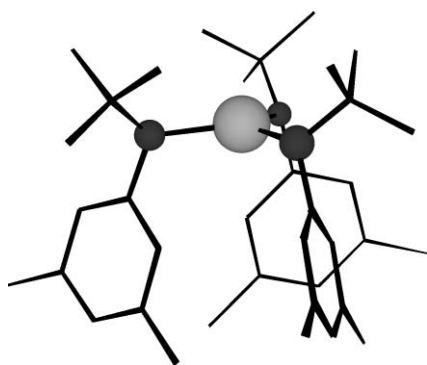


Fig. 1 $\text{Mo}[\text{N}(\text{R})\text{Ar}]_3$ complex ($\text{R} = \text{tBu}$, $\text{Ar} = 3,5\text{-C}_6\text{H}_3\text{Me}_2$).

The R group not only limits the size of the incoming molecules but also affects their reactivity once they are bound to $\text{Mo}[\text{N}(\text{R})\text{Ar}]_3$. Even relatively small changes in the size of the R group can result in very different products for the reaction of $\text{Mo}[\text{N}(\text{R})\text{Ar}]_3$ with N_2 . When the R substituent is large, for example when $\text{L} = \text{N}(\text{Ad})\text{Ar}$ or $\text{N}(\text{Ad})\text{Ph}$, the N_2 bridged dimer is not observed presumably due to steric crowding.¹⁴ When $\text{R} = \text{tBu}$, the reaction with N_2 produces $\text{N}(\text{tBu})\text{Mo}[\text{N}(\text{tBu})\text{Ar}]_3$, as outlined in previous studies,^{7,8} but when $\text{R} = \text{tPr}$, the nitride product $\text{N}(\text{tPr})\text{Mo}[\text{N}(\text{tPr})\text{Ar}]_3$ is not observed and instead the single atom-bridged complex, $[\text{Ar}(\text{tPr})\text{N}]_3\text{Mo}(\text{N})\text{Mo}[\text{N}(\text{tPr})\text{Ar}]_3$, is the major product.²⁴ For an even smaller ligand, $\text{L} = \text{N}(\text{Me})_2$, both the single atom-bridged complex, $\text{L}_3\text{Mo}(\text{N})\text{MoL}_3$, and the metal–metal bonded Mo_2L_6 dimer have been isolated.²⁵

In an earlier study we investigated the effect of the steric bulk of the $\text{N}(\text{R})\text{Ar}$ ligands on the structure and spin state of the intermediate dimer, $\text{N}_2\text{-}\{\text{Mo}[\text{N}(\text{R})\text{Ar}]_3\}_2$, but did not examine the overall reaction energetics or different reaction pathways.²⁶ There have been other computational studies of the effect of the ligands on N_2 activation in these complexes but these have been primarily concerned with the role of the ligand donor atom or metal.^{21,27} An earlier study by Hahn *et al.*²³ did investigate the steric influence of a variety of ligands in the N_2 cleavage reaction using molecular-mechanics. Their work confirmed that the main function of the bulky amide ligands was to screen the apical coordination site necessary for dinitrogen binding in order to prevent dimerisation of MoL_3 to form the stable metal–metal bonded Mo_2L_6 complex.

Although experimental work has shown that the nature of the $\text{N}(\text{R})\text{Ar}$ ligands has a profound effect on the outcome

of the reaction of MoL_3 complexes with N_2 , to date there has been no detailed study investigating the influence of both steric and electronic factors of the ligands on the competing reaction pathways. Accordingly, in the present study we make use of combined quantum-mechanical and molecular-mechanics (QM/MM) methods based on density functional theory (DFT) to explore the effect of the R group size in NR_2 and $\text{N}(\text{R})\text{Ar}$ ligands on the reaction energetics and resulting products. In particular, reaction pathways are explored for the formation of the nitrido product, $\text{L}_3\text{Mo}(\text{N})$, single atom-bridged complex, $\text{L}_3\text{Mo}(\text{N})\text{MoL}_3$, and metal–metal bonded dimer, Mo_2L_6 . Apart from the model system with $\text{L} = \text{NH}_2$, the other ligands involved in the calculations are those employed in experimental studies, namely $\text{L} = \text{NMe}_2$, $\text{N}(\text{tPr})\text{Ar}$ and $\text{N}(\text{tBu})\text{Ar}$. QM/MM methods are ideal for this investigation since they allow the important electronic parts of the molecule to be treated with DFT, while the remainder of the molecule can be efficiently dealt with using molecular mechanics.

Computational details

The calculations carried out in this work were performed using the Amsterdam Density Functional (ADF)^{28–30} program (2002 and 2004 versions) running on either Linux-based Pentium IV computers or the Australian National University Supercomputing Facility. All calculations used the local density approximation (LDA) to the exchange potential, the correlation potential of Vosko, Wilk and Nusair (VWN),³¹ the Becke³² and Perdew³³ corrections for non-local exchange and correlation, and the numerical integration scheme of te Velde and co-workers.³⁴ Geometry optimisations were performed using the gradient algorithm of Versluis and Ziegler.³⁵ All electron, triple- ζ Slater type orbital basis sets (TZP) with polarisation functions were used for all atoms. Relativistic effects were incorporated using the zero order relativistic approximation (ZORA).^{36–38} For the model structures, minima were confirmed by the absence of any imaginary frequencies, the latter being computed by numerical differentiation of energy gradients in slightly displaced geometries.^{39,40} All calculations were carried out in a spin-unrestricted manner. The convergence criteria for geometry optimisations were 10^{-3} Hartrees for energy and 10^{-2} Hartrees \AA^{-1} for gradient. SCF convergence was set at 10^{-6} . The integration parameter, accint, was set to 4.0 for geometry optimisations and to 6.0 for frequency calculations. For calculations on the experimental $\text{M}[\text{N}(\text{R})\text{Ar}]_3$ ($\text{R} = \text{Me}$, tPr , or tBu , $\text{Ar} = \text{Me}$, or $3,5\text{-C}_6\text{H}_3\text{Me}_2$) system, the QM/MM⁴¹ method implemented in ADF was used. For these calculations, the system was partitioned into two regions, one of which was treated with DFT and the other with molecular mechanics. The electronically important parts of the molecule, N_2 , the N donor atoms from the amide ligands, and Mo, were treated with DFT while the Me, tPr , tBu and $3,5\text{-C}_6\text{H}_3\text{Me}_2$ substituents were treated with molecular mechanics using the Sybyl⁴² force field available in ADF. UFF van der Waals parameters⁴³ were used for Mo while all other parameters involving the metal atoms were set to zero. The bonds that cross the QM/MM partition, known as link bonds, were “capped” by H for the QM region. The ratio of the link bond to the length of the capping bond was kept constant throughout the calculations corresponding to the link bond parameters being fixed at values of $\alpha_{(\text{N}-\text{C}(\text{R}))} = 1.489$ and $\alpha_{(\text{N}-\text{C}(\text{Ar}))} = 1.412$. This partitioning

Table 1 Calculated bond lengths and angles for MoL₃, N–MoL₃, Mo₂L₆ and L₃Mo–N–MoL₃ for L = NH₂, N(Me)₂, N(ⁱPr)Ar and N(^tBu)Ar. Full QM calculations in italics. Experimental values are included in parentheses where available

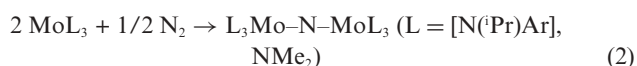
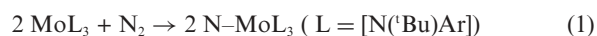
Complex	L	Bond length/Å			Bond angle/°	
		Mo–Mo	Mo–N	Mo–N _{amide}	Mo–N–Mo	Mo–N _L –C _R
MoL ₃	NH ₂			1.982		125
	NMe ₂			1.980		123
	<i>QM</i>			2.000		124
	N(ⁱ Pr)Ar			1.994		122
	<i>Cyclometallated</i>			1.993		129,130,78
				(1.927(6), 1.959(6), 1.987(6)) ²⁴		(132.7(5), 133.5(5), 78.6(4)) ²⁴
	N(^t Bu)Ar			2.004		122
N–MoL ₃	NH ₂		1.664	1.978		125
	NMe ₂		1.664	1.979		125
			1.669	1.995		127
	N(ⁱ Pr)Ar		1.666	1.987		122
			(1.640(4)) ²⁴	(1.973(4), 1.990(4), 1.999(4)) ²⁴		(126.3(4), 127.1(3), 127.3(3)) ²⁴
	N(^t Bu)Ar		1.666	1.989		126
	N(^t Bu)Ph		(1.658(5)) ⁸	(1.979(2)) ⁸		(128(2)) ⁸
Mo ₂ L ₆	NH ₂	2.240		1.990		127
	NMe ₂	2.254		1.986		129
		(2.214(3)) ⁴⁶		(1.98(1)) ⁴⁶		(133(2)) ⁴⁶
	N(ⁱ Pr)Ar	2.367		2.010		135
	N(^t Bu)Ar	2.466		2.054		141
L ₃ Mo–N–MoL ₃	NH ₂	3.658	1.829	1.978	180	123
	NMe ₂	3.669	1.834	1.981	180	120
			(1.7990(8)) ²⁵	(1.948(9), 1.953(8), 1.955(8)) ²⁵		
	N(ⁱ Pr)Ar	3.650	1.828	1.988	174	123
			(1.8204(4)) ²⁴	(1.968(4), 1.971(4), 1.971(4)) ²⁴	(180) ²⁴	(128.3(3), 126.9(3), 125.6(3)) ²⁴
	N(^t Bu)Ar	3.759	1.887	2.019	170	130

scheme is very similar to that used in the study of N₂O cleavage by Mo[N(R)Ar]₃.⁴⁴ All QM/MM calculations were undertaken in C₁ symmetry. Since it is not possible to confirm the nature of the minima from frequency calculations for the QM/MM calculations using ADF, a thorough exploration of all sensible ligand conformations was conducted to ensure that the optimised structures corresponded as close as possible to the global minimum geometry.

Results and discussion

Model system (L = NH₂)

Calculations were first carried out using a model system where the N(R)Ar ligands were replaced by NH₂, in order to compare the energetics for the different reaction pathways in the absence of steric strain. The three reactions under study, and the ligands, L, for which they are observed, are:



The lowest energy structures calculated for the single atom-bridged, [H₂N]₃Mo–N–Mo[NH₂]₃, and metal–metal bonded, [H₂N]₃Mo≡Mo[NH₂]₃, dimers are shown in Fig. 2. The structures of the reactant Mo[NH₂]₃, N₂ complex N₂–Mo[NH₂]₃, nitride product N–Mo[NH₂]₃, and intermediate dimer [H₂N]₃Mo–N₂–Mo[NH₂]₃, have already been reported in earlier work.²⁷ The

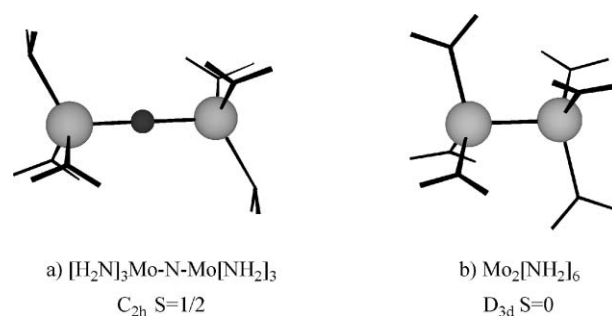


Fig. 2 Optimised structures of N–{Mo[NH₂]₃}₂ and [H₂N]₃Mo≡Mo[NH₂]₃.

relevant bond lengths and angles obtained from the calculations on these species are detailed in Table 1 along with the experimental values when known.

The single atom-bridged complex, N–{Mo[NH₂]₃}₂, is calculated to have a doublet ground state, consistent with the experimental data for L₃Mo–N–MoL₃ with N(ⁱPr)Ar.²⁴ The calculated Mo–N bond length of 1.829 Å in the Mo–N–Mo bridge is also in good agreement with the experimentally determined value of 1.8204(4) Å for (μ-N){Mo[N(ⁱPr)Ar]₃}₂.²⁴ The lowest energy structure has C_{2h} symmetry with one ligand rotated by 90° at each metal center (see Fig. 2). The ligand rotation is due to a Jahn–Teller distortion since in trigonal symmetry, an odd number of electrons occupy the doubly-degenerate HOMO involving the d_{xz} and d_{yz} orbitals on Mo. However, ligand rotation only stabilises the system by 15 kJ mol^{–1} compared to 56 kJ mol^{–1} for the N₂–{Mo[NH₂]₃}₂ intermediate dimer. As our earlier studies have

Table 2 Stabilization energy (E_s) of products relative to reactants for reactions 1 to 3 with $L = \text{NH}_2$

	$E_s/\text{kJ mol}^{-1}$
Reaction 1	-335
Reaction 2	-313
Reaction 3	-367

shown,²⁷ ligand rotation in the $\text{N}_2\text{-}\{\text{Mo}[\text{NH}_2]_3\}_2$ dimer greatly enhances the backdonation from the metal d orbitals to the π^* orbitals of N_2 , an effect which is not important for the single atom-bridged complex $\text{N-}\{\text{Mo}[\text{NH}_2]_3\}_2$.

The metal-metal bonded dimer $\text{Mo}_2[\text{NH}_2]_6$ is calculated to have a singlet ground state and a staggered conformation with D_{3d} symmetry, in accord with other experimental and computational studies.^{46,47} The Mo-Mo bond length of 2.240 Å is in reasonable agreement with the experimental value of 2.214(3) Å.⁴⁶ The barrier to rotation around the central Mo-Mo bond was estimated from a linear transit to be at most 13 kJ mol⁻¹ (data included in ESI†).

The energy of stabilization for the products relative to reactants are summarized in Table 2 for each reaction pathway. All three reactions are seen to be exothermic by at least 300 kJ mol⁻¹. Not surprisingly, in the absence of steric strain reaction 3, involving formation of the metal-metal bonded dimer, is the most thermodynamically favoured product. Since formation of the metal-metal bonded dimer is usually undesirable for small molecule activation, large R groups are used to prevent the metals approaching close enough to form a metal-metal bond. The calculated data place the strength of the Mo-Mo bond at 367 kJ mol⁻¹ for the model complex. This is in good agreement with the experimentally determined Mo-Mo bond strength of 398 ± 18 kJ mol⁻¹ for the $\text{Mo}_2[\text{NMe}_2]_6$ dimer⁴⁸ considering the differences between the model and experimental systems.

Of the two remaining reactions in Table 2, reaction 1 is about 20 kJ mol⁻¹ more exothermic than reaction 2, which raises the following question. If reaction 1 is more thermodynamically favourable, why does reaction 2 occur when $L = \text{N}(\text{Pr})\text{Ar}$? It has been proposed that in reaction 2, the nitride product does form first *via* reaction 1 but then goes on to form the single atom-bridged complex $\text{N-}\{\text{Mo}[\text{N}(\text{R})\text{Ar}]_3\}_2$ through reaction with any remaining starting material, $\text{Mo}[\text{N}(\text{R})\text{Ar}]_3$,²⁴ as shown in reaction 4:



The energy of reaction 4 can be readily determined from the energies already calculated for reactions 1 and 2, and is found to be exothermic by 146 kJ mol⁻¹, and therefore favourable. Reaction 4 was studied further by undertaking a linear transit in which one of the Mo-N bonds in $[\text{H}_2\text{N}]_3\text{Mo-N-Mo}[\text{NH}_2]_3$ was varied. The results are plotted in Fig. 3 for both the doublet and quartet spin states. Since $\text{Mo}[\text{NH}_2]_3$ has a quartet spin state and $\text{N-Mo}[\text{NH}_2]_3$ a singlet ground state, the reaction begins on the quartet surface but when the Mo-N distance is approximately 2.4 Å, the doublet surface crosses below the quartet to become the ground state. There is no barrier to the reaction in either spin state and since spin-orbit coupling is not insignificant for Mo^{III} , spin-crossover should be facile in these systems.

Although the reaction of $\text{Mo}[\text{NH}_2]_3$ with N_2 to form $\text{N-Mo}[\text{NH}_2]_3$ is thermodynamically favoured, any remaining starting

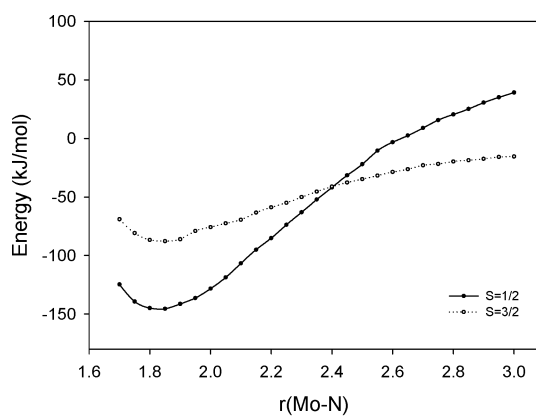
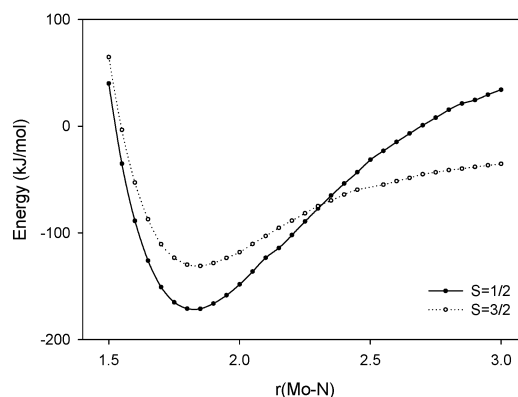
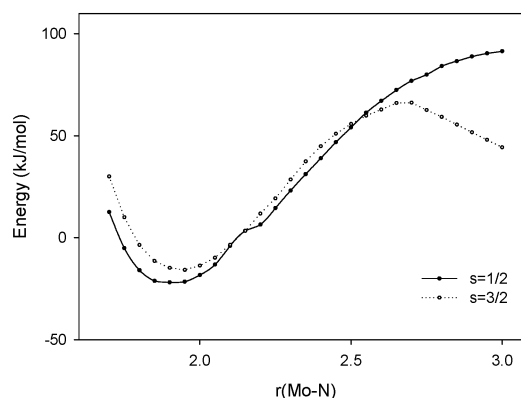
a) Formation of $\text{N-}\{\text{Mo}[\text{NH}_2]_3\}_2$ c) Formation of $\text{N-}\{\text{Mo}[\text{N}(\text{Pr})\text{Ar}]_3\}_2$ d) Formation of $\text{N-}\{\text{Mo}[\text{N}(\text{tBu})\text{Ar}]_3\}_2$

Fig. 3 Linear transit results for (a) $[\text{H}_2\text{N}]_3\text{Mo-N} + \text{Mo}[\text{NH}_2]_3 \rightarrow [\text{H}_2\text{N}]_3\text{Mo-N-Mo}[\text{NH}_2]_3$, (b) $[\text{Ar}(\text{Pr})\text{N}]_3\text{Mo-N} + \text{Mo}[\text{N}(\text{Pr})\text{Ar}]_3 \rightarrow [\text{Ar}(\text{Pr})\text{N}]_3\text{Mo-N-Mo}[\text{N}(\text{Pr})\text{Ar}]_3$, (c) $[\text{Ar}(\text{tBu})\text{N}]_3\text{Mo-N} + \text{Mo}[\text{N}(\text{tBu})\text{Ar}]_3 \rightarrow [\text{Ar}(\text{tBu})\text{N}]_3\text{Mo-N-Mo}[\text{N}(\text{tBu})\text{Ar}]_3$.

material, $\text{Mo}[\text{NH}_2]_3$, can react with either N_2 or $\text{N-Mo}[\text{NH}_2]_3$. In the latter case the reaction is 44 kJ mol⁻¹ less exothermic† but the first step in reaction 1, involving the uptake of N_2 by $\text{Mo}[\text{NH}_2]_3$ to form $[\text{H}_2\text{N}]_3\text{Mo-N}_2$, is only exothermic by approximately 70 kJ mol⁻¹²⁷ and experimentally is known to be

† To compare the two reactions, the enthalpy of reaction 4 must be doubled to 291 kJ mol⁻¹

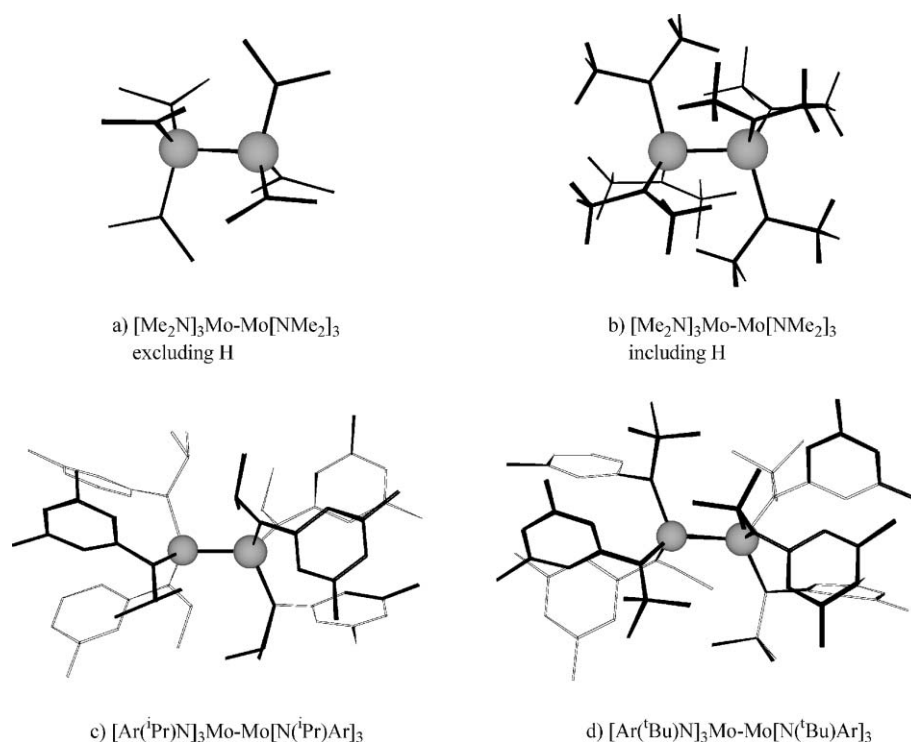


Fig. 4 Optimised Mo_2L_6 structures for $\text{L} = \text{NMe}_2$, $\text{N}(\text{iPr})\text{Ar}$ and $\text{N}(\text{tBu})\text{Ar}$.

slow for $\text{Mo}[\text{N}(\text{tBu})\text{Ar}]_3$.⁸ There is also a barrier to N–N cleavage in the $\text{L}_3\text{Mo}-\text{N}_2-\text{MoL}_3$ intermediate dimer of 66 kJ mol^{-1} for the model system²⁷ (97 kJ mol^{-1} for $\text{L} = \text{N}(\text{tBu})\text{Ar}$ from experimental studies).⁸ In comparison, there is no barrier to formation of $[\text{H}_2\text{N}]_3\text{Mo}-\text{N}-\text{Mo}[\text{NH}_2]_3$. Consequently, reaction 4 is kinetically favoured over reaction 1 and should be observed in conditions where there is an excess of the reactant.

Experimental systems ($\text{L} = \text{NMe}_2$, $\text{N}(\text{iPr})\text{Ar}$ and $\text{N}(\text{tBu})\text{Ar}$)

The energetics of reactions 1 to 4 were examined for the experimental ligand systems using QM/MM methods. Geometries were optimised for MoL_3 , $\text{N}-\text{MoL}_3$, $\text{N}-\{\text{MoL}_3\}_2$ and Mo_2L_6 with $\text{L} = \text{NMe}_2$, $\text{N}(\text{iPr})\text{Ar}$ and $\text{N}(\text{tBu})\text{Ar}$, and for $\text{N}_2-\{\text{MoL}_3\}_2$ with $\text{L} = \text{NMe}_2$. The structures of $\text{N}_2-\{\text{MoL}_3\}_2$ for $\text{L} = \text{N}(\text{iPr})\text{Ar}$ and $\text{N}(\text{tBu})\text{Ar}$ have been previously calculated in our earlier work.²⁶ Selected structural data for these complexes is given in Table 1 and the calculated structures shown in Fig. 4 and Fig. 5. In addition, full QM calculations were carried out on the reactant and product for $\text{L} = \text{NMe}_2$ in order to compare with the QM/MM results.

ML_3 and $\text{N}-\text{ML}_3$

$\text{Mo}[\text{NMe}_2]_3$ and $\text{N}-\text{Mo}[\text{NMe}_2]_3$ were calculated to have approximately D_{3h} and C_{3v} symmetry, respectively, for both QM/MM and full QM calculations. The calculated QM/MM bond lengths and angles are similar to those obtained for the model complexes, and in the case of $\text{L} = \text{NMe}_2$, are in excellent agreement with the full QM calculations.

The calculated structures for $\text{Mo}[\text{N}(\text{iPr})\text{Ar}]_3$, $\text{Mo}[\text{N}(\text{tBu})\text{Ar}]_3$, $\text{N}-\text{Mo}[\text{N}(\text{iPr})\text{Ar}]_3$ and $\text{N}-\text{Mo}[\text{N}(\text{tBu})\text{Ar}]_3$ all have approximately

C_3 symmetry and are similar to the $\text{Mo}[\text{N}(\text{tBu})\text{Ar}]_3$ and $\text{N}-\text{Mo}[\text{N}(\text{tBu})\text{Ph}]_3$ structures determined from X-ray crystallography with the R and Ar groups arranged on opposite sides of the MoN_3 plane.⁸ In general, the calculated bond distances and angles given in Table 1 are in good agreement with the crystallographically determined values. Although $\text{N}-\text{Mo}[\text{NMe}_2]_3$ has been synthesised, to date no crystal data have been reported,^{25,49} consequently, it is not possible to compare the calculated structures with experiment for this complex. $\text{Mo}[\text{NMe}_2]_3$ has been postulated as a transient in the reaction of $\text{N}-\text{Mo}[\text{NMe}_2]_3$ with $\text{Mo}[\text{N}(\text{tBu})\text{Ar}]_3$ ²⁵ but has not been observed experimentally presumably because the $\text{Mo}_2[\text{NMe}_2]_6$ dimer is far more stable.

Experimentally, the structure of $\text{Mo}[\text{N}(\text{iPr})\text{Ar}]_3$ is not known as ligation of Mo^{III} by $\text{N}(\text{iPr})\text{Ar}$ results in the cyclometallated complex $\text{Mo}(\text{H})(\eta^2-\text{Me}_2\text{C}=\text{NAr})(\text{N}(\text{iPr})\text{Ar})_2$ which then acts as a source of $\text{Mo}[\text{N}(\text{iPr})\text{Ar}]_3$ via a reversible cyclometallation process.²⁴ Since the QM/MM partition used in this study does not allow for a Mo–H bond, full QM calculations were undertaken on both $\text{Mo}(\text{H})(\eta^2-\text{Me}_2\text{C}=\text{NAr})(\text{N}(\text{iPr})\text{Ar})_2$ and $\text{Mo}[\text{N}(\text{iPr})\text{Ar}]_3$ in order to directly compare their stabilities. The calculated structure of $\text{Mo}(\text{H})(\eta^2-\text{Me}_2\text{C}=\text{NAr})(\text{N}(\text{iPr})\text{Ar})_2$ is shown in Fig. 6. From the full QM calculations, $\text{Mo}[\text{N}(\text{iPr})\text{Ar}]_3$ is predicted to have a quartet ground state and approximately C_3 symmetry, analogous to the QM/MM calculations, while $\text{Mo}(\text{H})(\eta^2-\text{Me}_2\text{C}=\text{NAr})(\text{N}(\text{iPr})\text{Ar})_2$ has a doublet ground state. The calculations reveal that the cyclometallated structure is stabilized by 24 kJ mol^{-1} relative to the trigonal structure which is in excellent agreement with the value of $21 \pm 8 \text{ kJ mol}^{-1}$ obtained from solution calorimetry studies.⁵⁰ From the experimental studies, the activation barrier to convert from the cyclometallated to the trigonal structure is similar, $19 \pm 2 \text{ kJ mol}^{-1}$.

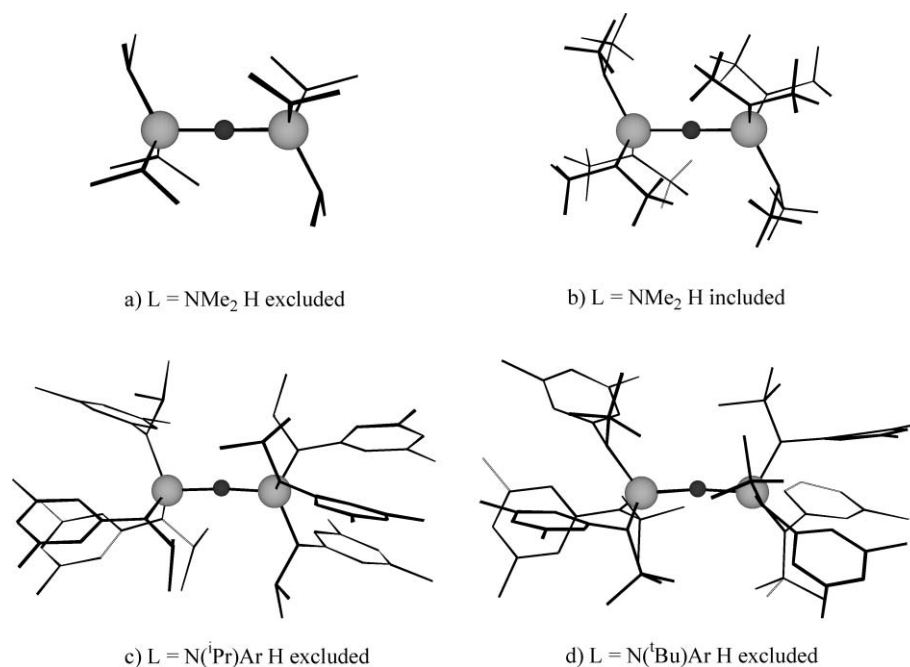


Fig. 5 Optimized QM/MM structures for $L_3\text{Mo-N-Mo}L_3$ for $L = \text{NMe}_2$, N^iPrAr , and N^tBuAr .

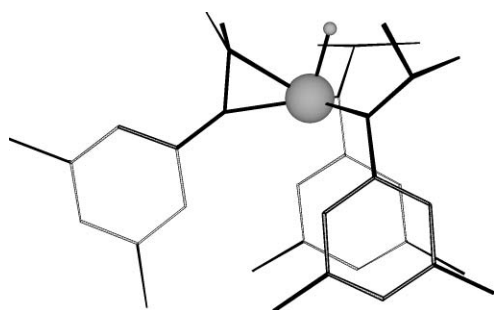


Fig. 6 QM optimised structure for $\text{Mo}(\text{H})(\eta^2\text{-Me}_2\text{C}=\text{NAr})(\text{N}^i\text{PrAr})_2$.

Mo_2L_6

The optimised structures for Mo_2L_6 are shown in Fig. 4 for $L = \text{NMe}_2$, N^iPrAr and N^tBuAr . $\text{Mo}_2[\text{NMe}_2]_3$ is calculated to have a staggered conformation with approximately D_{3d} symmetry, very similar to the calculated model structure and the experimentally determined solid state structure which has approximately D_{3d} symmetry.⁴⁶ The calculated structures for $L = \text{N}^i\text{PrAr}$ and N^tBuAr also have approximately staggered geometries, although the size of the ligands prevent the dimer from forming the “ideal” staggered conformation. The Mo_2L_6 dimer is not known for $L = \text{N}^i\text{PrAr}$ and N^tBuAr , presumably because the steric bulk of the ligands prevents the metals from approaching close enough to form a metal–metal bond.

$L_3\text{Mo-N-Mo}L_3$

The optimised structures of the single atom-bridged complex $L_3\text{Mo-N-Mo}L_3$ for $L = \text{NMe}_2$, N^iPrAr and N^tBuAr are shown in Fig. 5. The calculated structure for $L = \text{NMe}_2$ has C_{2h} symmetry and is similar to the model system with a staggered conformation and one ligand rotated by 90° at each

metal centre. Again, as found for the M_2L_6 structures, for the larger N^iPrAr and N^tBuAr ligands, $\text{N}-\{\text{Mo}L_3\}_2$ cannot achieve the ideal staggered conformation due to the steric crowding of the R groups. Furthermore, whereas the calculated structure for $L = \text{NMe}_2$ has a linear Mo-N-Mo core, the structures for $L = \text{N}^i\text{PrAr}$ and N^tBuAr are bent with Mo-N-Mo angles of 174° and 170° , respectively.

The $(\mu\text{-N})\{\text{Mo}[\text{NMe}_2]_3\}_2$ and $(\mu\text{-N})\{\text{Mo}[\text{N}^i\text{PrAr}]_3\}_2$ complexes have been synthesised and structurally characterised by X-ray crystallography.^{24,25} Both structures have the bridging nitrogen atom at an inversion center and approximately trigonal symmetry. Although no ligand rotation was observed in either structure, disorder of the $\text{Mo}[\text{NMe}_2]_3$ moiety around the threefold axis is observed in the related complex $[\text{Me}_2\text{N}]_3\text{Mo-N-Mo}[\text{N}(\text{R})\text{Ar}_F]_3$ and was accounted for by rotation of the NMe_2 ligands.²⁵

General comments on structures

In general, the calculated Mo-N , $\text{Mo-N}_{\text{amide}}$ and Mo-Mo bond lengths increase as the ligands increase in size, consistent with increasing steric crowding as the R groups become larger. Not surprisingly, the Mo-Mo bond lengths in Mo_2L_6 show the greatest increase with R group size. There is a 10% increase in the Mo-Mo bond length on going from $L = \text{NH}_2$ to N^tBuAr compared to an increase of approximately 3% in the Mo-N and Mo-Mo distances in $L_3\text{Mo-N-Mo}L_3$. For Mo_2L_6 and $\text{N}-\{\text{Mo}L_3\}_2$, the $\text{Mo-N}_L\text{-C}_R$ bond angles also increase with increasing size of the R group. These results are in agreement with the MM results reported in the study by Hahn *et al.*²³

The calculated Mo-Mo distance for $\text{N}-\{\text{Mo}[\text{N}^t\text{BuAr}]_3\}_2$ is 3.759 \AA . Since this complex has not been experimentally observed, the N^tBuAr ligands must prevent the metals from approaching any closer than 3.76 \AA . For the larger bridging atom, P, formation of the single-atom bridged complex is favourable as the related

Table 3 Reaction enthalpies (kJ mol⁻¹) for reactions 1 to 4 with L = NH₂, N(ⁱPr)Ar and N(^tBu)Ar calculated using QM/MM methods. Since a comparative QM/MM value for Mo(H)(η²-Me₂C=NAr)(N(ⁱPr)Ar)₂ is not possible, the energy of trigonal Mo[N(ⁱPr)Ar]₃ is used instead, with the result that the enthalpies for the reactions involving L = N(ⁱPr)Ar are overestimated by approximately 24 kJ mol⁻¹

	Reaction 1	Reaction 2	Reaction 3	Reaction 4 ^a
L	2 MoL ₃ + N ₂ → 2 N–MoL ₃	2 MoL ₃ + 1/2 N ₂ → L ₃ Mo–N–MoL ₃	2 MoL ₃ → Mo ₂ L ₆	2 MoL ₃ + 2N–MoL ₃ → 2L ₃ Mo–N–MoL ₃
NH ₂	–335	–313	–367	–291
N(Me) ₂	–344	–348	–403	–351
N(ⁱ Pr)Ar	–317	–331	–227	–344
N(^t Bu)Ar	–293	–167	+78	–41

^a Note: In order to compare with reaction 1, reaction 4 has been doubled.

[Ph(^tBu)N]₃Mo–P–Mo[N(^tBu)Ph]₃ complex has been isolated and structurally characterized with a Mo–Mo distance of 4.486 Å.²⁵ For L = N(ⁱPr)Ar, the calculated Mo–Mo distance for N–{MoL₃}₂ is 3.650 Å. Thus, the change from R = ⁱPr to R = ^tBu makes a significant difference to the steric crowding between the metal centers, making it possible for N–{Mo[N(ⁱPr)Ar]₃}₂ to form.

Reaction energetics

The calculated enthalpies for reactions 1 to 4 are summarised in Table 3 for L = NH₂, NMe₂, N(ⁱPr)Ar, and N(^tBu)Ar. Overall, the exothermicity of each reaction decreases as the ligand size increases from NMe₂ through to N(^tBu)Ar. This trend can be largely attributed to increased steric crowding in the products compared to the reactants for each reaction.

Ligand size has the greatest effect on reaction 3, where the enthalpy of reaction changes from exothermic by 403 kJ mol⁻¹ for L = NMe₂, to endothermic by 78 kJ mol⁻¹ for L = N(^tBu)Ar. Although reaction 3 is exothermic by 227 kJ mol⁻¹ for L = N(ⁱPr)Ar, to date the formation of Mo₂[N(ⁱPr)Ar]₆ has not been reported experimentally. To explore the possibility of a kinetic barrier to its formation, a linear transit was undertaken. These calculations, which employed broken symmetry methods⁵¹ to allow for antiferromagnetic coupling between the metal centres at long Mo–Mo distances, revealed no significant barrier to the formation of Mo₂[N(ⁱPr)Ar]₆. Based on these results and the calculated exothermicity for this reaction of 227 kJ mol⁻¹, Mo₂[N(ⁱPr)Ar]₆ is expected to form readily from Mo[N(ⁱPr)Ar]₃. However, cyclometallation of Mo[N(ⁱPr)Ar]₃ discussed earlier is intramolecular and expected to be fast relative to intermolecular dimerisation and may be responsible for preventing Mo₂[N(ⁱPr)Ar]₆ formation.

Overall, the formation of N–{MoL₃}₂ from reaction 2 is favourable for all ligands used in this study, even though it is unknown experimentally when L = N(^tBu)Ar. However, reaction 2 can be broken down into two parts; the first step is the reaction of MoL₃ with N₂ to form N–MoL₃ *via* reaction 1, and the second step is the reaction of N–MoL₃ with remaining MoL₃ to form L₃Mo–N–MoL₃ *via* reaction 4. For L = NMe₂ and N(ⁱPr)Ar, reaction 4 is very exothermic and the single atom-bridged complex is the thermodynamically favoured product. For L = N(^tBu)Ar, reaction 4 is only exothermic by 41 kJ mol⁻¹ compared to 293 kJ mol⁻¹ for reaction 1. Consequently, for this ligand reaction 1 is now the thermodynamically more favourable pathway.

To gain a better understanding of the ligand dependence of these reactions, in particular, to obtain estimates for any kinetic

barriers to bond formation or cleavage, linear transits were carried out for the formation of N–{MoL₃}₂ (reaction 4) for both L = N(ⁱPr)Ar and N(^tBu)Ar and the results plotted in Fig. 3. The linear transit curves for (μ-N){Mo[N(ⁱPr)Ar]₃}₂ are similar to those calculated for the model system. The reaction begins on the quartet surface and crosses to the doublet at approximately 2.3 Å (*cf.* 2.4 Å for the model system) and there is no barrier to the formation of (μ-N){Mo[N(ⁱPr)Ar]₃}₂ in either spin state. In experiment, Mo(H)(η²-Me₂C=NAr)(N(ⁱPr)Ar)₂ and not Mo[N(ⁱPr)Ar]₃ would be the reactive species but since Mo(H)(η²-Me₂C=NAr)(N(ⁱPr)Ar)₂ cannot be modelled with the QM/MM partition employed in this study, Mo[N(ⁱPr)Ar]₃ is used instead. As discussed previously, this replacement introduces an error of at most 24 kJ mol⁻¹. For L = N(^tBu)Ar, the reaction also begins on the quartet surface and crosses to the doublet at a Mo–N distance of about 2.5 Å, but unlike the reaction for L = N(ⁱPr)Ar, there is now a barrier to formation of 66 kJ mol⁻¹ in the quartet state. There is no barrier in the doublet state but the quartet state lies below the doublet for Mo–N distances longer than 2.5 Å. Although this barrier is surmountable at room temperature or above, the reaction is only exothermic by 21 kJ mol⁻¹, compared to 293 kJ mol⁻¹ for reaction 1.

In summary, the presence of a kinetic barrier to the formation of L₃Mo–N–MoL₃ in reaction 4 combined with the low exothermicity, results in reaction 1 being the preferred pathway for L = N(^tBu)Ar, accounting for why the single-atom bridged species is not observed experimentally for this ligand. For L = N(ⁱPr)Ar, however, there is no barrier to formation of L₃Mo–N–MoL₃, and it is also the thermodynamically favoured product. Since the uptake of N₂ to form the dimer N₂–{Mo[N(^tBu)Ar]₃}₂ is known to be slow experimentally in the absence of a catalyst,⁸ reaction 4 is both the kinetically and thermodynamically favoured pathway for this ligand.

One unexpected result from Table 3 is that reaction 4 is more exothermic for L = NMe₂ and N(ⁱPr)Ar than for L = NH₂, despite the increase in ligand size. The increased exothermicity of reaction 4 for these larger ligands appears to be associated with ligand rotation in the structure of the L₃Mo–N–MoL₃ complex which relieves some of the steric crowding around the metal center. The stabilisation gained by allowing the ligands to rotate away from a trigonal arrangement around the metal centres is 35 kJ mol⁻¹ for L = N(ⁱPr)Ar compared to only 6 kJ mol⁻¹ for the L = NH₂ system. Since ligand rotation is not observed in N–Mo[N(R)Ar]₃ or Mo[N(R)Ar]₃ for any of the R groups studied, this extra stabilisation only applies to the L₃Mo–N–MoL₃ complex and hence increases the exothermicity of the reaction. This is

Table 4 The QM and MM contributions to the QM/MM energy for $L_3Mo-N-MoL_3$, $L = N(^iPr)Ar$ and $N(^iBu)Ar$. The QM energy of the optimised model system, $L = NH_2$, is included for comparison

Energy/kJ mol ⁻¹	NH ₂	N(^iPr)Ar	N(^iBu)Ar
QM	-11 702	-11 653	-11 593
MM	—	-40	+62

consistent with earlier work where we found that ligand rotation in $[Ar(R)N]_3Mo-N_2-Mo[N(R)Ar]_3$ ⁵² is more favourable for $L = N(^iPr)Ar$ and $N(^iBu)Ar$ than for the model system.

The change in ligand from $L = N(^iPr)Ar$ to $N(^iBu)Ar$ results in a dramatic shift in the exothermicity of reaction 3 from -344 to -41 kJ mol⁻¹. To rationalize this difference, the QM and MM contributions to the overall QM/MM energy are given in Table 4 for both ligands along with the QM energy for the model system.

The MM component of the energy stabilizes the system by 40 kJ mol⁻¹ for $L = N(^iPr)Ar$ but destabilizes the system by 62 kJ mol⁻¹ for $L = N(^iBu)Ar$. The additional MM stabilisation for $L = N(^iPr)Ar$ is mostly due to ligand rotation, as discussed earlier. The fact that the bond lengths and angles for $L = N(^iPr)Ar$ in Table 1 are quite similar to those for $L = NH_2$, suggests that the $N(^iPr)Ar$ ligand can be accommodated in the $L_3Mo-N-MoL_3$ complex without large changes in geometry. In contrast, the longer $Mo-N$ bond lengths and more distorted ligand orientations in Table 1 for $L = N(^iBu)Ar$ compared to $L = NH_2$ and $N(^iPr)Ar$ indicate that most of the destabilising MM energy arises from steric crowding between the two metal centers.

In the QM/MM partition used in this study, the QM region is identical to the model system used in Section 2.1. Any variation in the QM energy for $L = N(^iPr)Ar$ and $N(^iBu)Ar$ relative to that of the optimised model system can thus be attributed to the electronic effect of changes in the $N_3Mo-N-MoN_3$ core geometry when the large bulky ligands are included. From Table 4 the energy of the QM region is 49 kJ mol⁻¹ and 109 kJ mol⁻¹ less stable than the model system for $L = N(^iPr)Ar$ and $N(^iBu)Ar$, respectively. This destabilization relative to the model system indicates that the $L_3Mo-N-MoL_3$ complex adopts a geometry that minimises steric crowding but is not as electronically favourable for the $N_3Mo-N-MoN_3$ core. This effect is more pronounced for larger ligands and therefore the barrier to formation is greatest for $L = N(^iBu)Ar$. Since the MM energy is destabilizing for $L = N(^iBu)Ar$ and the QM energy is comparatively less stabilizing, the reaction is far less favourable than for $L = N(^iPr)Ar$ where the destabilization of the QM contribution is approximately cancelled by the stabilizing MM contribution.

Although the above analysis explains why the overall reaction energetics are different for $L = N(^iPr)Ar$ and $N(^iBu)Ar$, it does not explain why the activation barrier is so much larger for $L = N(^iBu)Ar$. To address this issue, it is worthwhile examining the reaction surface for the formation of $L_3Mo-N-MoL_3$. Since this complex has a rotated ligand structure whereas L_3Mo-N and MoL_3 both have trigonal geometries, one ligand at each metal center must rotate during the formation of $L_3Mo-N-MoL_3$. A comparison of the calculated structures of $L_3Mo-N + MoL_3$ along the reaction profile shows that for $Mo-N$ distances between 2.4 and 2.7 Å, ligand rotation does occur for $L = N(^iBu)Ar$. For $L = N(^iPr)Ar$ however, the ligands are much closer to a trigonal arrangement. The rotation of the $N(^iBu)Ar$ ligand reduces the

steric crowding but is electronically unfavourable for the $N_3Mo-N-MoN_3$ core at these $Mo-N$ bond lengths. As a result, the system is destabilized and the activation barrier significantly larger.

Conclusions

Calculations were carried out on the reaction pathways involving the formation of L_3Mo-N , $L_3Mo-N-MoL_3$ and Mo_2L_6 complexes for $L = NH_2$, NMe_2 , $N(^iPr)Ar$ and $N(^iBu)Ar$ in order to rationalize the different products resulting from a change in the ligand, L . In general, the exothermicity of each reaction decreases as the ligand size increases from NMe_2 through to $N(^iBu)Ar$, and this trend can be largely attributed to increased steric crowding in the products compared to reactants. The formation of the metal-metal bonded dimer *via* reaction 3 ($2 MoL_3 \rightarrow Mo_2L_6$) is the most exothermic pathway in the absence of steric strain. However, the enthalpy of this reaction changes dramatically with ligand size, changing from -403 kJ mol⁻¹ for $L = NMe_2$ to +78 kJ mol⁻¹ for $L = N(^iBu)Ar$.

Of the remaining pathways, reaction 1 ($N_2 + 2 MoL_3 \rightarrow 2 N-MoL_3$) is thermodynamically favoured over reaction 2 ($1/2 N_2 + 2 MoL_3 \rightarrow L_3Mo-N-MoL_3$) by 22 kJ mol⁻¹ for the model system. The latter reaction is thought to occur through the formation of $N-MoL_3$ from reaction 1, followed by the reaction of $N-MoL_3$ with any remaining MoL_3 *via* reaction 4 ($L_3Mo-N + MoL_3 \rightarrow L_3Mo-N-MoL_3$). However, the uptake of N_2 by MoL_3 in reaction 1 to form $L_3Mo-N_2-MoL_3$ is known to be slow experimentally,⁸ and furthermore, the overall barrier to $N-N$ cleavage is calculated at 66 kJ mol⁻¹ for the model system. In contrast, reaction 4 is calculated to be barrierless and therefore is kinetically favoured over reaction 1.

For $L = NMe_2$ and $N(^iPr)Ar$, reaction 4 is calculated to be more exothermic than reaction 1 and, since there is no barrier to the formation of $L_3Mo-N-MoL_3$ for both ligands, it is both the thermodynamically and kinetically favoured pathway resulting in $L_3Mo-N-MoL_3$ as the main product, in agreement with experiment. However, when $L = N(^iBu)Ar$, reaction 4 is only exothermic by 21 kJ mol⁻¹ and has a barrier of approximately 66 kJ mol⁻¹. Consequently, for $L = N(^iBu)Ar$, reaction 1 is favoured both thermodynamically and kinetically over reaction 2, resulting in $N-MoL_3$ as the major product, again consistent with experimental findings.

Acknowledgements

The authors greatly acknowledge the Australian Research Council for financial support in the form of an Australian Postgraduate Award for G. C. and a Discovery Project Grant for R. S. and B. F. Y. (DP0663045). The National Science Foundation of the USA is acknowledged for funding support (CHE-0316823) to C. C. C. The Australian National University is also acknowledged for access to the APAC (Australian Partnership for Advanced Computing) supercomputing facilities.

References

- 1 M. D. Fryzuk and S. A. Johnson, *Coord. Chem. Rev.*, 2000, **200**–202, 379–409.
- 2 M. D. Fryzuk, *Chem. Rec.*, 2003, **3**(1), 2–11.
- 3 M. P. Shaver and M. D. Fryzuk, *Adv. Synth. Catal.*, 2003, **345**(9–10), 1061–1076.

- 4 D. V. Yandulov and R. R. Schrock, *Science*, 2003, **301**(5629), 76–78.
- 5 D. V. Yandulov, R. R. Schrock, A. L. Rheingold, C. Ceccarelli and W. M. Davis, *Inorg. Chem.*, 2003, **42**(3), 796–813.
- 6 A. E. Shilov, *Russ. Chem. Bull.*, 2003, **52**(12), 2555–2562.
- 7 C. E. Laplaza and C. C. Cummins, *Science*, 1995, **268**, 861–863.
- 8 C. E. Laplaza, M. J. A. Johnson, J. C. Peters, A. L. Odom, E. Kim, C. C. Cummins, G. N. George and I. J. Pickering, *J. Am. Chem. Soc.*, 1996, **118**, 8623–8638.
- 9 P. W. Wanandi, W. M. Davis, C. C. Cummins, M. A. Russell and D. E. Wilcox, *J. Am. Chem. Soc.*, 1995, **117**(7), 2110–2111.
- 10 A. L. Odom, C. C. Cummins and J. D. Protasiewicz, *J. Am. Chem. Soc.*, 1995, **117**(24), 6613–6614.
- 11 S. L. Stokes, W. M. Davis, A. L. Odom and C. C. Cummins, *Organometallics*, 1996, **15**(21), 4521–4530.
- 12 K. B. P. Rupp, N. Desmangles, S. Gamberotta, G. Yap and A. L. Rheingold, *Inorg. Chem.*, 1997, **36**(6), 1194–1197.
- 13 J. P. F. Cherry, A. R. Johnson, L. M. Baraldo, Y. C. Tsai, C. C. Cummins, S. V. Kryatov, E. V. Rybak-Akimova, K. B. Capps, C. D. Hoff, C. M. Haar and S. P. Nolan, *J. Am. Chem. Soc.*, 2001, **123**, 7271–7286.
- 14 J. C. Peters, J. P. F. Cherry, J. C. Thomas, L. Baraldo, D. J. Mindiola, W. M. Davis and C. C. Cummins, *J. Am. Chem. Soc.*, 1999, **121**(43), 10053–10067.
- 15 C. E. Laplaza, W. M. Davis and C. C. Cummins, *Organometallics*, 1995, **14**(1), 577–580.
- 16 M. G. Fickes, A. L. Odom and C. C. Cummins, *Chem. Commun.*, 1997, (20), 1993–1994.
- 17 A. L. Odom, P. L. Arnold and C. C. Cummins, *J. Am. Chem. Soc.*, 1998, **120**, 5836–5837.
- 18 A. Furstner, C. Mathes and C. W. Lehmann, *J. Am. Chem. Soc.*, 1999, **121**(40), 9453–9454.
- 19 D. J. Mindiola, K. Meyer, J. P. F. Cherry, T. A. Baker and C. C. Cummins, *Organometallics*, 2000, **19**, 1622–1624.
- 20 Y. C. Tsai and C. C. Cummins, *Inorg. Chim. Acta*, 2003, **345**, 63–69.
- 21 Q. Cui, D. G. Musaev, M. Svensson, S. Sieber and K. Morokuma, *J. Am. Chem. Soc.*, 1995, **117**, 12366–12367.
- 22 K. M. Neyman, V. A. Nasluzov, J. Hahn, C. R. Landis and N. Rösch, *Organometallics*, 1997, **16**, 995–1000.
- 23 J. Hahn, C. R. Landis, V. A. Nasluzov, K. M. Neyman and N. Rösch, *Inorg. Chem.*, 1997, **36**(18), 3947–3951.
- 24 Y. C. Tsai, M. J. A. Johnson, D. J. Mindiola, C. C. Cummins, W. T. Klooster and T. F. Koetzle, *J. Am. Chem. Soc.*, 1999, **121**(44), 10426–10427.
- 25 M. J. A. Johnson, P. M. Lee, A. L. Odom, W. M. Davis and C. C. Cummins, *Angew. Chem., Int. Ed. Engl.*, 1997, **36**(1–2), 87–91.
- 26 G. Christian, R. Stranger, B. F. Yates and D. C. Graham, *Dalton Trans.*, 2005, (5), 962–968.
- 27 G. Christian, J. Driver and R. Stranger, *Faraday Discuss.*, 2003, **124**, 331–341.
- 28 G. te Velde, F. M. Bickelhaupt, E. J. Baerends, C. Fonseca Guerra, S. J. A. Van Gisbergen, J. G. Snijders and T. Ziegler, *J. Comput. Chem.*, 2001, **22**(9), 931–967.
- 29 C. Fonseca Guerra, J. G. Snijders, G. Te Velde and E. J. Baerends, *Theor. Chem. Acc.*, 1998, **99**(6), 391–403.
- 30 Theoretical Chemistry, *Amsterdam Density Functional (ADF)*, SCM, Vrije Universiteit, Amsterdam, The Netherlands, 2002, <http://www.scm.com>.
- 31 S. H. Vosko, L. Wilk and M. Nusair, *Can. J. Phys.*, 1980, **58**(8), 1200–1211.
- 32 A. D. Becke, *Phys. Rev. A*, 1988, **38**(6), 3098–3100.
- 33 J. P. Perdew, *Phys. Rev. B*, 1986, **33**(12), 8822–8824.
- 34 G. T. Velde and E. J. Baerends, *J. Comput. Phys.*, 1992, **99**(1), 84–98.
- 35 L. Versluis and T. Ziegler, *J. Chem. Phys.*, 1988, **88**(1), 322–328.
- 36 E. van Lenthe, E. J. Baerends and J. G. Snijders, *J. Chem. Phys.*, 1993, **99**(6), 4597–4610.
- 37 E. van Lenthe, E. J. Baerends and J. G. Snijders, *J. Chem. Phys.*, 1994, **101**(11), 9783–9792.
- 38 E. van Lenthe, A. Ehlers and E. J. Baerends, *J. Chem. Phys.*, 1999, **110**(18), 8943–8953.
- 39 L. Y. Fan and T. Ziegler, *J. Phys. Chem.*, 1992, **96**(17), 6937–6941.
- 40 L. Y. Fan and T. Ziegler, *J. Chem. Phys.*, 1992, **96**(12), 9005–9012.
- 41 T. K. Woo, L. Cavallo and T. Ziegler, *Theor. Chem. Acc.*, 1998, **100**(5–6), 307–313.
- 42 M. Clark, R. D. Cramer and N. Vanopdenbosch, *J. Comput. Chem.*, 1989, **10**(8), 982–1012.
- 43 A. K. Rappe, C. J. Casewit, K. S. Colwell, W. A. Goddard and W. M. Skiff, *J. Am. Chem. Soc.*, 1992, **114**(25), 10024–10035.
- 44 D. V. Khoroshun, D. G. Musaev and K. Morokuma, *Organometallics*, 1999, **18**(26), 5653–5660.
- 45 C. E. Laplaza, A. L. Odom, W. M. Davis, C. C. Cummins and J. D. Protasiewicz, *J. Am. Chem. Soc.*, 1995, **117**(17), 4999–5000.
- 46 M. H. Chisholm, F. A. Cotton, B. A. Frenz, W. W. Reichert, L. W. Shive and B. R. Stults, *J. Am. Chem. Soc.*, 1976, **98**(15), 4469–4476.
- 47 T. Ziegler, *J. Am. Chem. Soc.*, 1983, **105**(26), 7543–7549.
- 48 F. A. Adedeji, K. J. Cavell, S. Cavell, J. A. Connor, G. Pilcher, H. A. Skinner and M. T. Zafarani-Moattar, *J. Chem. Soc., Faraday Trans. 1*, 1979, **75**, 603–613.
- 49 J. C. Peters, A. R. Johnson, A. L. Odom, P. W. Wanandi, W. M. Davis and C. C. Cummins, *J. Am. Chem. Soc.*, 1996, **118**, 10175–10188.
- 50 F. H. Stephens, J. S. Figueroa, C. C. Cummins, O. P. Kryatova, S. V. Kryatov, E. V. Rybak-Akimova, J. E. McDonough and C. D. Hoff, *Organometallics*, 2004, **23**(13), 3126–3138.
- 51 L. Noodleman and J. G. Norman, *J. Chem. Phys.*, 1979, **70**(11), 4903–4906.
- 52 G. Christian, R. Stranger and B. F. Yates, *Inorg. Chem.*, 2006, **45**(17), 6851–6859.